14th Australasian Fluid Mechanics Conference
Adelaide University, Adelaide, Australia
10-14 December 2001

Impulsively started flow over an airfoil at an angle of attack

K. Parker[1], J. Soria[1], T. T. Lim[2] and T. H. New[2]

[1]Laboratory for Turbulence Research in Aerospace & Combustion
Monash University, Melbourne, 3800 AUSTRALIA

[2]Department of Mechanical Engineering
National University of Singapore, 119260 SINGAPORE

Abstract

This paper reports on a preliminary study undertaken to investigate the evolution and structure of flow accelerated from a stationary state over a NACA 0015 airfoil at an angle of attack of 30^o. The results from two uniform accelerations of 50 mm/s^2 and 100 mm/s^2 are presented. In both cases the final uniform velocity was 100 mm/s. The Reynolds number based on this uniform velocity and the chord length of the airfoil was 8000. PIV measurements were conducted to measure the in-plane velocity field and the out-of-plane vorticity evolution around the airfoil. These measurements have revealed a rich and complex unsteady flow structure. The observable dispersion of vorticity seen in both acceleration cases is indicative of the unsteady 3-D nature of the flow. The results show that the evolution of the dynamic stall vortex is retarded in the faster acceleration case.

Introduction

Unsteady viscous flows past lifting surfaces have significant engineering applications and have been the centre of much research over the decades. More specifically, impulsively started unsteady viscous flow past lifting surfaces is important in aircraft takeoff and landing scenarios, helicopter rotor dynamic stall and turbomachinery operating in unsteady regimes. The major thrust in unsteady airfoil research has been directed at understanding and predicting non-linear phenomenon, that are beyond the scope of classical thin-airfoil theory. To date, most studies have focused on 2-dimensional airfoils. For example, McCroskey [8] and Carr [2] focused on the unsteady flow effects in dynamic stall. Basu [1] investigated the case of a 2-D airfoil in an unsteady pitching motion and was able to predict the lift and drag numerically. Later studies by Chow [3] and Katz [7] used a discrete vortex method to investigate impulsive flow past an airfoil. Similarly, Morikawa & Gronig [9] have investigated the relationship between leading edge vortex development around a NACA 0015 airfoil at an angle of attack of 30^o and its effect on the aerodynamic forces at $Re = 35,000$, based on chord and final steady free-stream velocity. Another form of unsteadiness that studies have focussed on is airfoils in pure heaving or pitching motion or combination of heave and pitch motion [10]. Qualitative smoke flow visualisation of unsteady oscillatory flow by Zaman [11] show the interactions of the dynamic stall vortex (DSV) and the trailing edge vortex. Freymuth [5] has also conducted a parametric study of the constant acceleration flow past a NACA 0015 airfoil at angles of attack up to 60^o, providing information of the complex vortical structure through flow visualizations. Although early studies have provided valuable information about the flow structures, many aspects of the flow field remain unclear, in particular the temporal variation of the velocity and vorticity fields. The lack of these information led us to the present investigation. The aim is to investigate the effect of acceleration on the flow over a NACA 0015 airfoil at an angle of attack of 30^o using PIV technique measurements. The flow is established from a zero-flow state and accelerated over a finite time. Of interest is the vortical interactions that occur in the transient evolutionary process that is prevalent. To do this, we made use of high resolution digital single exposed imaging with multigrid cross-correlation digital particle image velocimetry (MC-CDPIV) [6] analysis to provide quantitative 2-component 2-dimensional (2C-2D) velocity field. In all cases, the acceleration of the flow is uniform.

Experimental Apparatus

The experiments were conducted in a recirculating water tunnel driven by a square piston. Figure 1 shows a schematic drawing of the water tunnel layout. The 2-Dimensional NACA 0015 airfoil, which has an aspect ratio (width/chord) of 2.5, spans the entire test section of the water tunnel. The airfoil was supported at 20 mm from the leading edge in the centre of the test section via a rotational mechanism that allows easy setting of the angle of attack from outside the water tunnel. All results presented in this paper are for an angle of attack of 30^o. The Reynolds number, which is based on an airfoil chord of 80 mm and the steady post-acceleration flow velocity of 100 mm/s, is equal to 8000. The static stall angle of attack for this airfoil is 16^o.

Initially the water in the tunnel is at rest, and the flow in the test section is accelerated using a piston driven by a stepper motor that is capable of 10,000 micro-steps per revolution at a maximum speed of 4 revolutions per second. The square face piston measures 200 $mm \times 200$ mm. A lead screw with 25 mm pitch, which is directly connected to the piston at one end and is connected via a coupling to the stepper motor at the other end, is used to convert the rotational motion into linear motion that moves the square piston.

The stepper motor is driven by a 2D88M driver controlled using TTL pulses from the parallel port of a *Real Time* Linux (RTLinux) PC. The stepper motor control program allows different piston acceleration profiles to be implemented. This operating system is capable of controlling the timing of the stepper motor pulses to better than 0.1 μs. The motion control signal from the RTLinux PC was acquired using a Data Translation 2838 data acquisition card to establish the accuracy of the motion of the stepper motor and hence, the accuracy of the programmed piston motion. Full details of the experimental set-up are presented in reference [6]. A typical displacement profile is shown in Figure 1. The corresponding velocity and acceleration profiles, obtained from the first

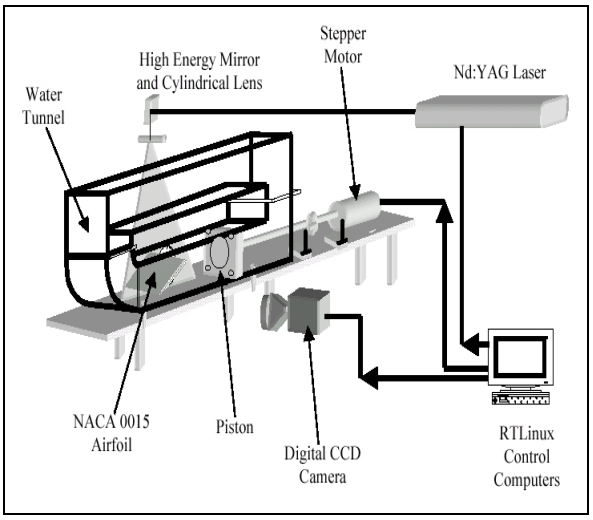

Figure 1: Arrangement of the recirculating water tunnel, NACA 0015 airfoil at a 30^0 angle of attack, the Nd:YAG laser, high resolution digital CCD camera and the associated control processors.

and second temporal derivatives of the displacement profile, are also shown. Note that the data is for an acceleration time of 1 s and acceleration of a = 100 mm/s^2. Two acceleration cases are presented in this paper:

• CASE I: a = 50 mm/s^2 with a uniform acceleration time $t_a = 2$ s.

• CASE 2: a = 100 mm/s^2 with a uniform acceleration time $t_a = 1$ s.

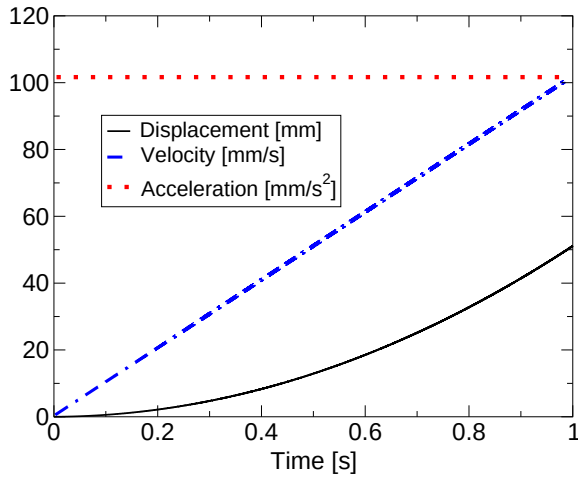

Figure 2: Piston displacement, velocity and acceleration history determined from the TTL pulses sent to the stepper motor.

Prior to the PIV experiments, the flow was uniformly seeded with Optimage particles (Powder No. 1), nominally 30 μm in diameter and with a density of 1000±20 kg/m^3. The illumination source for the recording of PIV images is a Continuum Nd:YAG twin cavity laser system capable of producing 2 × 200 mJ pulses of 6 ns duration at 10 Hz. A cylindrical lens was used to expand the laser beam into a 2 mm light sheet.

The scattered light from the seed particles was recorded on a Kodak ES4.0 12 bit digital CCD camera, which has an array size 2048 px × 2048 px. This digital camera can be operated in double-shutter mode for single exposed PIV image recording. The image pair recordings were made at the maximum acquisition frequency of 2.5 image pairs per second (i.e. 400 ms between image pairs). A 105 mm Micro-Nikkor lens set at an aperture of $f2.8$ and at a reproduction ratio of 5 was used for all experiments. With these settings, and assuming aberation-free optics, the estimated depth of field for these experiments was 0.7 mm and the diffraction limited particle image size was 7.4 μm ($i.e.$ $1.2px$). Further details of the MCCDPIV analysis can be found in [6].

Results and Discussion

Figure 3 shows the velocity and vorticity field at $t' = t/t_a = 0.2$, just after start-up. The figure is applicable for both acceleration cases of 50 mm/s^2 and 100 mm/s^2. At this time it would appear that the boundary layer is still fully attached to the airfoil in both cases and the flow is in a laminar state. Flow direction is indicated from left to right. The in-plane vector field is coloured by the out-of-plane vorticity which is taken as positive out of the page. The legend below each image indicates the vorticity value.

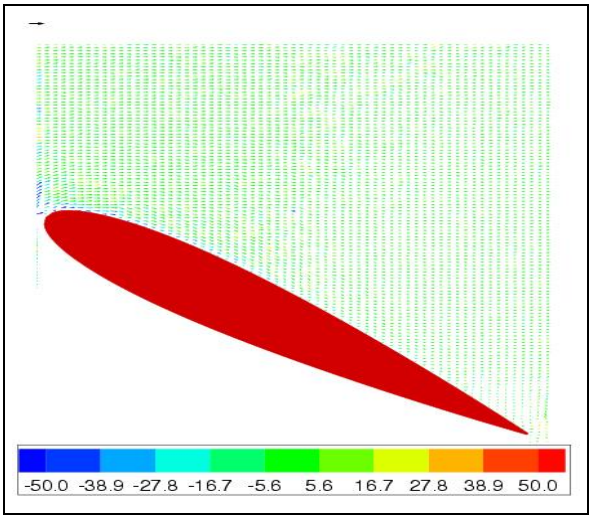

Figure 3: Non-dimensional velocity and vorticity field for CASE I and II at $t' = t/t_a = 0.2$.

Figure 4 shows the temporal evolution of the unsteady flow for a constant piston acceleration $a = 50$ mm/s^2 which lasts for a duration $t_a = 2$ s. The 4 frames represent the post-acceleration phase of the flow at $t' = t/t_a = 0.8, 1.2, 1.6,$ and 1.8 respectively. Due to limitations imposed by the PIV acquisition rate, the data does not shed any light on the possible similarity of the flow structures during the acceleration phase. Similarly, figure 5 shows the corresponding PIV results for a constant piston acceleration $a = 100$ mm/s^2 over $t' = 0.8, 1.2, 1.6$ and 1.8.

At $t' = 0.8$ in figure 4(a) it appears that there is initial growth of surface vorticity at the leading edge of the airfoil. This area is indicated by the small region of concentrated vorticity at the leading edge of the airfoil. Comparatively, in figure 5(a) the same region appears smaller in size. The vorticity appears to be spread more

evenly along the upper surface of the airfoil.

At $t' = 1.2$ the vortical structure appears larger for CASE I in figure 4(b) than for CASE II in figure 5(b). In both cases the shear layer appears to have rolled up from the previous image at $t' = 0.8$ as a result of an increasing pressure gradient. At this time the airfoil appears to have entered light stall given that the boundary layer region has grown to a thickness of the order of the airfoil thickness. At $t' = 1.6$ in figure 4(c) the leading edge vortex, which has clockwise circulation, appears to have increased in size and continues to convect further downstream of the leading edge of the airfoil. In the region just below the larger vortical structure and the airfoil upper surface, a smaller structure with circulation opposite in direction to the larger structure, appears to form from another shear layer. The two structures form a counter-rotating pair of vortices on the upper surface. At this time this is not yet visible in figure 5(c) for CASE II.

At $t' = 1.8$ in figure 4(d) the centre of the larger vortical structure has moved out of the field of view. The flow appears complex with a number of small vortical structures interacting with each other. The flow is characterised by a relatively wide wake in the region above the trailing edge which is simialr in thickness to the airfoil chord length. This may be indicative of dynamic stall [8]. Unlike the dynamic stall phenomenon observed by Panda et al [10] and Zaman et al [11] where both a DSV and a trailing edge vortex was visible, only the DSV is observed here. However, their experiments dealt with an airfoil in pure pitching oscillations which may account for the trailing edge vortex.

In figure 5(d), at $t' = 1.8$ the vortical structure is still not fully seperated from the airfoil. At this time the smaller vortical structure with opposite circulation seen in figure 4(b) is present. It appears that the airfoil is approaching deep stall. In both cases, at later times ($t' = 1.6, 1.8$ and 2.0), the observable dispersion of vorticity is indicative of the unsteady, complex and 3-D nature of the flow. The non-uniform and random distribution of vorticity seen in these figures may suggest significant out-of-plane velocity gradients which have a contracting and stretching effect on the vortices. There appears to be instabilities in the shear layer that look like "Kelvin- Helmholtz-type" roll-ups. The evolution (creation, growth and convection) of vorticity appears to take longer when the flow has greater acceleration.

Although the evolution of the gross features in CASE I are similar to CASE II once the uniform velocity regimes are established, one observable difference is that generally the vortical structures in CASE II appear more compact and well defined than for CASE I. In the higher acceleration case the increased fluid momentum the greater velocity fgradient increases the creation of vorticity at the leading edge and have an effect of stretching the vortices in the direction of the main flow. This action has another effect of retarding any growth of the structures. These results are unexpected since one would expect that increase flow acceleration would cause the structures to evolve quicker. An alternative to using u_∞/a_∞ to scale the evolution time is $\sqrt{c/a_\infty}$, where a_∞ = acceleration, u_∞ = velocity and c = airfoil chord length. It is felt that the vortical development has a greater dependancy on the flow acceleration and airfoil chord than the flow velocity. If this method is used, figure 4(a) and 5(b) would be compared at $t' = 0.42$, figure 4(b) and 5(c) correspond to $t' = 0.57$ and figure 4(c) and 5(d) are comparable at time $t' = 0.63$. These comparisons indicate greater similarity of the structures in time and space.

Conclusions

A preliminary study has been undertaken to investigate the effect of uniform acceleration on the evolution and structure of the separated flow around a NACA 0015 airfoil at an angle of attack of 30^o. High resolution single exposed image recording with multigrid cross-correlation PIV analysis has revealed a complex flow topology of this flow. This study has also found that larger flow acceleration leads to more compact and more intense separated shear layer and vortical regions. This scenario may apply only during early stages of the flow evolution and may not be manifested at larger times. The study has observed the DSV within the evolutionary process which occurs widely in space and time. Scaling the evolution times with the flow acceleration instead of the velocity results in comparison of images that look more similar. This issue is being investigated further.

References

[1] Basu, B. C. & Hancock, G. J., The unsteady motion of a two-dimensional aerofoil in incompressible inviscid flow. *J. Fluid Mech.*, **27**, 1978, 159-178.

[2] Carr, L., Progress in analysis and prediction of dynamic stall, *J. of Aircraft*, **25**(1), 1988, 6-17.

[3] Chow, S. N., The initial lift and drag of an impulsively started airfoil of finite thickness.*J. Fluid Mech.*, **118**, 1981, 393-409.

[4] Fouras, A. & Soria, J., Accuracy of out-of-plane vorticity measurements using in-plane velocity vector field data. *Exp. Fluids*, **25**, 1998, 409-430.

[5] Freymuth, P., The vortex patterns of dynamic separation: a parametric and comparative study. *Progress in Aerospace Sciences*, **22**, 1985, 161-208.

[6] Soria, J., Lim, T. T., Parker, K. & New, T. H., Investigation of accelerated flow over an airfoil at an angle of attach using multigrid cross-correlation digital PIV. In *4th International Symposium on Particle Image Velocimetry*, Gottingen, Germany, 2001.

[7] Katz, A discrete vortex method for the non-steady separated flow over an airfoil. *J. Fluid Mech.*, **102** , 1981, 315-328.

[8] McCroskey, W. J., Unsteady Airfoils, *Ann. Rev. Fluid Mech.*, **24**, 1982, 285-311.

[9] Morikawa, K. & Gronig, H., Formation and structure of vortex systems around a translating and oscillating airfoil. *Z. Flugwiss. Welraumforsch.*, **19**, 1995, 391-396.

[10] Panda, J., Zaman, K. B. M. Q. & Kim, S. W., Numerical investigation of unsteady translational flow over an oscilating airfoil formation and structure of vortex systems around a translating and oscillating airfoil. *ASME: J. Fluids Eng.*, **117**, 1995, 10-19.

[11] Zaman, K. B. M. Q. & Panda, Experimental investigation of the flow field of an oscillating airfoil and estimation of lift from wake surveys. *J. Fluid Mech.*, **265**, 1994, 65-95.

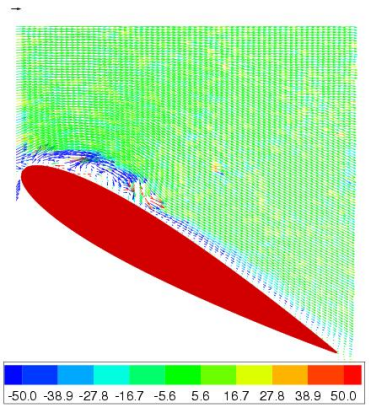

(a)

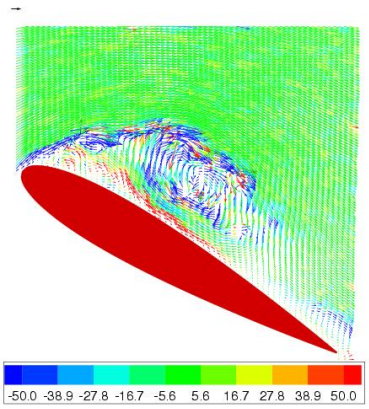

(b)

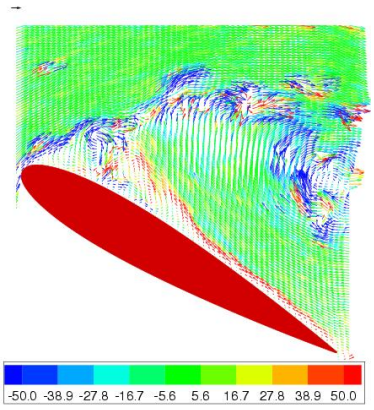

(c)

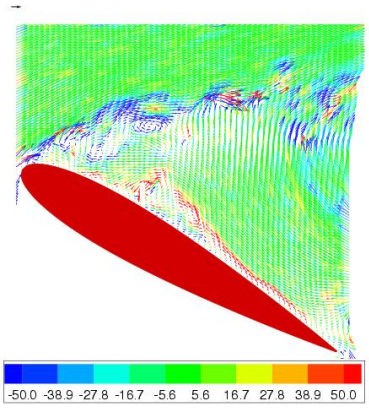

(d)

Figure 4: Non-dimensional velocity and vorticity fields for the uniform acceleration case of a = 50 mm/s^2. The evolution is down the page. The data is shown for times of 0.8, 1.2, 1.6 and 1.8 (time is non-dimensionalised by $t_a = u_\infty/a_\infty = 2\ s$).

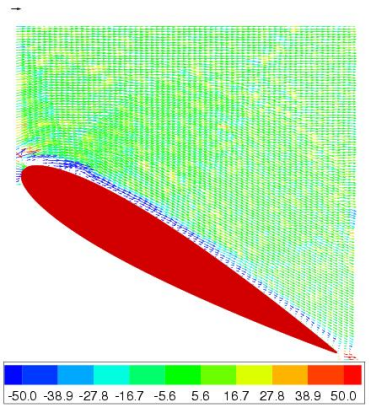

(a)

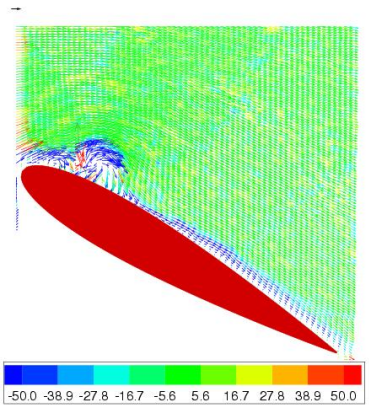

(b)

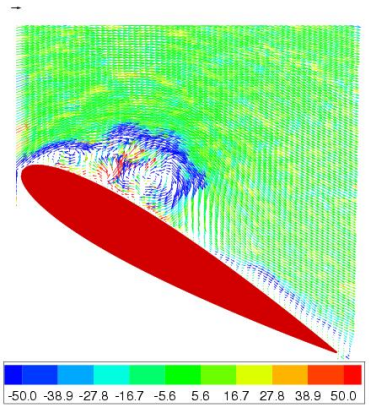

(c)

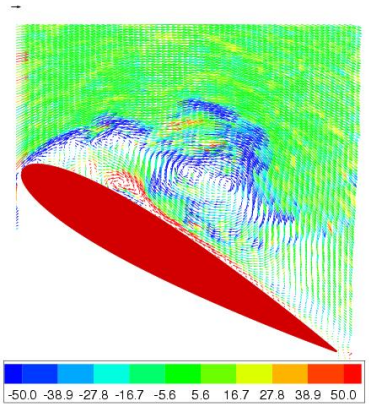

(d)

Figure 5: Non-dimensional velocity and vorticity fields for the uniform acceleration case of a = 100 mm/s^2. The evolution is down the page. The data is shown for times of 0.8, 1.2, 1.6 and 1.8 (time is non-dimensionalised by $t_a = u_\infty/a_\infty = 1\ s$).